Remote Sensing of Environment 168 (2015) 194–204

Contents lists available at ScienceDirect

Remote Sensing of Environment

journal homepage: www.elsevier.com/locate/rse

Landsat-based mapping of thermokarst lake dynamics on the Tuktoyaktuk Coastal Plain, Northwest Territories, Canada since 1985

Ian Olthof *, Robert H. Fraser, Carla Schmitt

Canada Centre for Remote Sensing, Natural Resource Canada, 560 Rochester, Ottawa, ON K1A 0E4, Canada

ARTICLE INFO

Article history:
Received 6 January 2015
Received in revised form 7 April 2015
Accepted 1 July 2015
Available online 20 July 2015

Keywords:
Landsat
Arctic
Thermokarst
Lake

ABSTRACT

Several remote sensing studies have documented widespread thermokarst lake expansion in continuous permafrost regions of North America over the past few decades. Other studies have found no long-term trends in water body extents, but large intra- and inter-annual changes driven by precipitation. These differences could be due to geographic variability in physical conditions (geology, climate, permafrost and hydrology) or in the data and methods used to extract water bodies. This study tested water extraction methods over the Tuktoyaktuk Coastal Plain, Northwest Territories (NWT), Canada, based on the Landsat 5 shortwave infrared (SWIR) channel and validated them using water extents obtained from 0.5 m resolution orthophoto imagery. Methods included applying thresholds to generate binary land/water classifications, as well as deriving 30 m water fractions from both linear unmixing and a new histogram breakpoint method. Results indicated that the histogram breakpoint method outperformed other methods, underestimating overall water fraction by 0.26% and overestimating the number of pure 30 m water pixels by 0.66% compared to water fractions calculated from orthophotos. The breakpoint method was then applied to a stack of 17 near peak-of-season Landsat 5 and Landsat 7 images acquired between July 4 and August 18 from 1985 to 2011 to create a water fraction time-series for examining both trends and inter-annual variation in water extent. Results showed an overall expansion of lake area along margins by 55 km^2 with isolated lakes experiencing rapid drainage totalling 15 km^2, leading to a net water area increase of 40 km^2 over the 26-year period.

1. Introduction

Surface water dynamics play an important role in physical, geochemical and biological processes that affect wildlife, water supply, transportation, and energy balance in Arctic regions (Vincent et al., 2013). Thermokarst lakes are the result of thawing permafrost or massive ground ice in Arctic regions where climate warming has been greatest in recent decades (Serreze et al., 2000). Rising ground temperatures have accelerated thermokarst processes and features such as thaw lakes in some Arctic regions (Jones et al., 2011; Kokelj & Jorgenson, 2013). Thus, surface water mapping and monitoring are becoming increasingly important to document these changes and provide insight into their underlying processes. To this end, a suite of recent studies have used remotely sensed imagery to map thermokarst lake extents and their changes in various regions across the Arctic and sub-Arctic (Jones et al., 2011; Plug et al., 2008; Roach et al., 2013; Rover et al., 2012; Smith et al., 2005). In general, these studies suggest that thermokarst lakes have increased in abundance and surface area in regions of continuous permafrost and decreased in transitional permafrost zones (discontinuous, isolated, sporadic) in Siberia, Alaska and Canada's Yukon and Northwest Territories. A broader synoptic analysis of lake changes across Canada from 250 m MODIS data between 2000–2009 revealed similar trends in the west, but widespread surface water losses in continuous permafrost further east in Canada's Nunavut Territory (Carroll et al., 2011).

While some general observations have been made on thermokarst lake dynamics in continuous permafrost regions, a number of authors have reported different directional changes. Smith, Sheng, MacDonald and Hinzman (2005) compared thirty-eight Landsat MSS scenes acquired in 1973 with Russian RESURS-1 satellite data acquired in 1997 and 1998 to report a net 12% increase in lake area in Siberia, while Riordan et al. (2006) found only negligible changes from 1950 to 2001 in continuous permafrost regions of Alaska using a combination scanned panchromatic and color airphotos, and satellite data from Landsat TM and ETM+. Plug, Walls and Scott (2008) used six Landsat MSS, TM and ETM+ scenes acquired in pairs across three decades to determine no significant long-term changes in lake area on the Tuktoyaktuk Peninsula between 1978 and 2001, but explained inter-annual variation by cumulative precipitation in the preceding year. Several authors have reported both lake expansion and drainage occurring simultaneously in continuous permafrost regions, and the relative importance of each process determines the net change in overall surface water extent and balance between carbon release and uptake (Walter

* Corresponding author.
E-mail address: Ian.Olthof@NRCan.gc.ca (I. Olthof).

http://dx.doi.org/10.1016/j.rse.2015.07.001
0034-4257/

Anthony et al., 2014). For example, on the Northern Seward Peninsula in Alaska, Jones et al. (2011) compared historical aerial photography with recent 1 m Ikonos imagery and found that although the number of water bodies increased by 10.7% between 1950 and 2006 and persistent water bodies grew incrementally around shorelines, overall water area decreased by 14.9% due to sudden drainage of a number of large lakes. Some of the inconsistencies among lake change studies may be explained by a lack of a common underlying process due to regional differences in physical geography, variability in observation frequency, or simply by a low sensitivity of methods used to extract lake area in relation to changes in lake extents.

To capture changes in Arctic lake extents, a number of different remote sensing data types and approaches have been used. Some studies have employed sub-meter resolution imagery including aerial photography to assess fine-scale shoreline changes (Jones et al., 2011; Sannel & Brown, 2010). While these analyses can extend back in time before digital satellite imagery, they tend to be limited by the number of available image dates, which can lead to mistaken conclusions due to a number of factors. First, anomalous climate events such as precipitation occurring before the satellite image is acquired can cause variability in water balance and lake size that may not reflect the overall longer-term trend (Chen et al., 2014; Plug et al., 2008). Second, false changes may be introduced by misregistration or spatial resolution scaling errors caused by different sensor characteristics between dates. And third, when few dates are used, the most common change detection approach involves classifying each date independently and assessing changes by comparing the resulting maps. This method, referred to as post-classification comparison, can lead to wrong conclusions due to the known fact that change error is the product of the errors of the two input classifications (Singh, 1989). Fortunately, classification errors tend to be relatively low for water. For example, Frazier and Page et al. (2000) reported a 96.9% overall accuracy classifying water bodies on riverine floodplains using Landsat TM, which would produce a 9% change error when assessed against a comparably accurate classification from a different time period. This level of error may exceed the level of change taking place, causing a low sensitivity of the method to accurately detect real water body changes. To improve change detection accuracy, certain authors have increased statistical power by applying trend detection on many observations arranged in a satellite image time-series. This approach has the advantage of being able to map underlying long-term processes while minimizing the influence of intra-annual variation due to phenology, changing atmospheric conditions and short-term changes in water balance (Chen et al., 2014; Roach et al., 2013; Rover et al., 2012). The application of robust regression for trend detection also minimizes the effects of georeferencing errors in a single year by treating misregistered observations as noise or outliers.

Systematic acquisition of satellite digital imagery began in 1972 for Landsat with the MSS sensor and in 1982 for Landsat TM/ETM+, offering repeatable imagery every 16 days to present. The USGS opened its entire Landsat archive to the public in 2008, enhancing the capacity to study regional-scale land/water dynamics and providing justification to re-analyze some regions with a greater number of satellite observations. Landsat TM/ETM+ offers the potential to monitor lake dynamics over the past three decades; however, its 30 m spatial resolution provides less precision than air photos or high resolution satellite imagery for examining lake extent changes. Spectral unmixing approaches have been used to increase precision by mapping sub-pixel water fractions from coarse resolution data including AVHRR (Hope et al., 1999) and MODIS (Sun et al., 2011; Weiss & Crabtree, 2011). Most Landsat studies have relied on hard binary classification approaches that map pixels as either water or land (Roach et al., 2012; Plug et al., 2008) with a few notable exceptions that have mapped percent water (Ji et al., 2008; Rover et al., 2010).

The current study explores three Landsat-based approaches for extracting surface water extent and changes over the Tuktoyaktuk Coastal Plain (TCP), NWT. First, we assess and compare the three methods against water maps derived from high resolution orthophotos. Second, we develop a calibrated Landsat image time-series over the TCP and apply the best method to produce a series of water maps from 1985 to 2011 for analysis. Finally, we examine inter-annual variability separate from long-term trends to map persistent water body changes and ephemeral water.

Objectives:

1. Compare a shortwave infrared (SWIR) thresholding approach to generate hard, binary water vs land classifications with linear and histogram breakpoint unmixing methods that classify fractional water extent within pixels.
2. Using the best mapping method, examine long-term trends and inter-annual variability in lake area on the Tuktoyaktuk Coastal Plain from 1985 to 2011.
3. Extend previous Landsat-based water change studies in continuous permafrost to Northwestern Canada to determine if lakes are behaving similarly among regions.

2. Methods

2.1. Study area

The study area covers a large portion of the Tuktoyaktuk Coastal Plain ecoregion, which includes the Tuktoyaktuk Peninsula (Fig. 1). The region is entirely within the zone of continuous permafrost (Heginbottom et al., 1995) with 10% or more ice content, creating landforms characteristic of periglacial environments such as ice wedge polygons, thaw slumps and pingos (Burn & Kokelj, 2009). Shallow lakes and ponds are numerous along the Tuktoyaktuk Peninsula where surficial geology consists mainly of colluvial, alluvial and lacustrine deposits (Rampton, 1987), generally becoming larger and less abundant (Fulton, 1995) to the south, where surficial geology consists mainly of till veneer and till blanket. Streams and rivers are nearly absent (Mackay, 1988), occurring primarily on floodplains and deltas that occupy a small percentage of the overall region.

The study area is almost entirely above the treeline with a few pockets of stunted white spruce in the southeast of the region within the treeline transition zone. Above treeline, vegetation is nearly continuous and consists mainly of erect shrubs, heath shrubs, cotton-grass tundra and non-vascular lichen and moss species on ice-wedge polygons. Mean annual temperature was approximately −9.5 °C from 1985 to 2011, with an average of 125 days with daily temperatures above freezing according to Environment Canada climate data for Tuktoyaktuk (Latitude: 69.43°; Longitude: −133.03°). The western Arctic of North America has experienced some of the most rapid climate warming on earth over the last 40 years (Serreze et al., 2000). At Tuktoyaktuk, winter temperatures have increased more than summer temperatures since 1985 (0.84 °C summer (June–August); 1.96 °C winter (December–February)). Mean annual ground temperatures in the region have increased by 1–3 °C since 1970 in association with rising air temperature (Burn & Kokelj, 2009). This warming was likely the cause of some of the most significant greening in Canada's Arctic (Pouliot, Latifovic & Olthof, 2009) primarily from shrub expansion, with associated declines in lichen cover (Fraser et al., 2014).

2.2. Data

2.2.1. Orthophotos

Digitally scanned, natural color orthophoto images acquired in August 2004 were obtained from the Mackenzie Valley Air Photo (MVAP) Project of the Government of the Northwest Territories Centre for Geomatics. Five orthophotos located south of the community of Tuktoyaktuk, each covering approximately 10 km × 10 km at 0.5 m spatial resolution, were used to validate Landsat-based water extraction

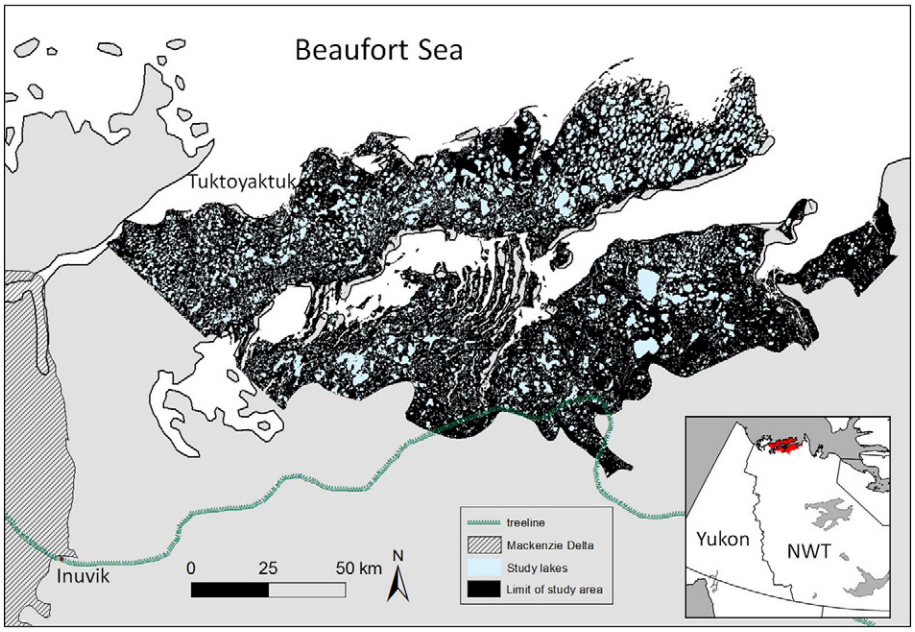

Fig. 1. Entire thermokarst lake study area covering a large portion of the Tuktoyaktuk Coastal Plain including the Tuktoyaktuk Peninsula.

methods. No absolute measure of geodetic accuracy is reported in the metadata; however, a visual check of several lakes located in different parts of each orthophoto revealed excellent alignment with Landsat with no visual offset.

Lakes were extracted from the GeoTIFF orthoimages using Adobe Photoshop CS4. The raster seeding tool was used to delineate approximately 20–25 lakes per image on a lake-by-lake basis. Raster seeding grows and fills in homogeneous regions based on color similarity to a seed pixel that is manually selected. Multiple seeds were sometimes needed to infill lakes completely in cases where several colors were present due to shallow bathymetry or suspended sediment. Effort was made to select dark homogeneous lakes and quality control was an important part of the process to ensure accurate shoreline delineation. A 3×3 mode filter was applied to the initial lake mask to remove noise and a sieve filter used to exclude objects within lakes less than 15 pixels in size. The final lake mask was subsequently buffered to a minimum of 60 m to create a land mask around each lake that would enable calculation of 30 m resolution mixed pixels containing different percentages of water and land. Each lake's land mask was quality checked and adjusted to ensure that no water was present in the form of ice wedge polygons or other thermokarst features. A total of 113 lakes covering a range of sizes between 8477 m^2 and 1,476,900 m^2 were extracted in this manner with land masks surrounding each (Fig. 2).

From the fine resolution lake and land masks, separate fraction images were generated showing the percentage of 0.5 m water and land pixels located in each 30 m pixel aligned with the Landsat grid. This was performed by locating the center of each Landsat pixel in the 0.5 m resolution lake/land mask image and calculating the number of each type within the surrounding 61×61 pixel window as a percentage of the window size (3721 pixels). Pixels located along the edge of a mask whose 30 m land and water fractions did not sum to 100% were removed.

2.2.2. Landsat

Seventeen Landsat 5 and Landsat 7 scenes were obtained from the USGS Glovis data archive representing years from 1985 to 2011, and WRS Path/Row 62/11. Scenes were terrain corrected Level 1 T with geodetic accuracies of one quarter to less than half a pixel. To minimize intra-annual hydrologic variability, anniversary dates were selected to represent mid-summer conditions on the Tuktoyaktuk Peninsula as closely as possible between early July and mid-August (Table 1). Landsat 7 scenes containing gaps caused by the post-2003 scanline correction failure were avoided to ensure the most complete coverage possible. Scenes were screened to remove cloud and cloud shadow and converted to Top-of-Atmosphere (TOA) reflectance using coefficients in the header file following Chander et al. (2009). Landsat SWIR 5 TOA images were stacked to form cubes with dimensions x and y representing space and dimension z representing time.

Trends were analyzed under two different area masks to facilitate their investigation.

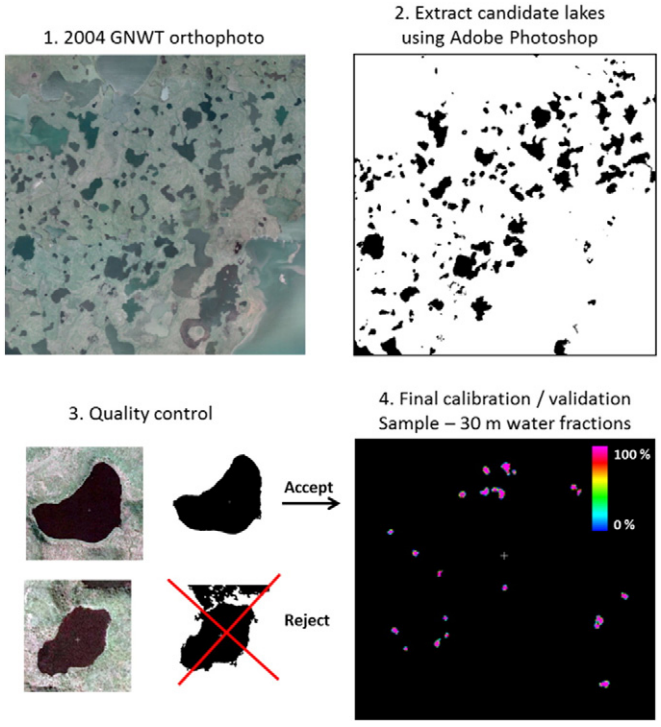

Fig. 2. Overview of methodology applied to one of five 0.5 m resolution scanned digital orthophotos used to generate 30 m water fractions from for 113 reference lakes.

Table 1
Landsat scenes by sensor and date for WRS Path/Row 62/11 used to examine water changes on the Tuktoyaktuk Peninsula. The 2004 scene in bold was used to validate Landsat water extraction methods.

Sensor	Date
Landsat 5 TM	August 7, 1985
Landsat 5 TM	August 10, 1986
Landsat 5 TM	July 14, 1988
Landsat 5 TM	August 18, 1989
Landsat 5 TM	July 4, 1990
Landsat 5 TM	July 25, 1992
Landsat 5 TM	July 28, 1993
Landsat 7 ETM +	August 6, 1999
Landsat 7 ETM +	July 23, 2000
Landsat 7 ETM +	July 13, 2002
Landsat 5 TM	July 26, 2004
Landsat 5 TM	August 14, 2005
Landsat 5 TM	August 1, 2006
Landsat 5 TM	August 4, 2007
Landsat 5 TM	July 5, 2008
Landsat 5 TM	July 27, 2010
Landsat 5 TM	July 14, 2011

1. A full study area mask (12,946 km^2) containing a varying number of Landsat observations from 17 dates (Table 1) for investigation of 1985–2011 water fraction trends (Fig. 1). This mask was buffered 300 m from ocean shorelines to minimize the effect of sea level and tapped lakes with direct connection to the ocean.
2. A mask representing 90% of the full study region mask (11,596 km^2) where consistent clear-sky coverage for 10 dates permits investigation of inter-annual variability in water fractions.

2.3. Landsat-based water extraction methods

The Landsat shortwave infrared (SWIR) band 5 has been shown to separate water from land better when used alone than in combination with other bands (Frazier and Page, 2000; Roach et al., 2012). Shortwave infrared radiation is strongly absorbed by water and is minimally affected by atmospheric aerosols, suspended sediment or plant material. A typical frequency distribution of SWIR 5 water and surrounding land is bi-modal, with one mode at the dark end of the histogram corresponding to water and the other on the bright end corresponding to land. Both modes are separated by pixels that represent varying mixtures of land and water. The range of the histogram brighter than the brightest pure water pixels and darker than the darkest pure land pixels defines the SWIR 5 spectral range associated with mixed land/water pixels, hereafter referred to as the 'mixed pixel region' (Fig. 3).

2.3.1. Hard threshold classification

A binary water/land classification was generated using a SWIR 5 threshold applied to the July 26, 2004 Landsat scene. SWIR pixel values equal to or below the threshold were assigned to water while those above were classified as land assuming no mixed pixels. The threshold was initially set to DN < = 26, which represented the SWIR 5 brightness with the minimum frequency in the mixed pixel region between water and land and was subsequently adjusted to maximize agreement between orthophoto and Landsat water fractions.

2.3.2. LLS unmixing

The radiance received by a sensor is the sum of the reflectance of pure materials within its field of view weighted by the fraction each material occupies. Pure materials are referred to as endmembers whose reflectance may be represented by a spectral signature that is unique to that material. If weighting is linear and the reflectance of each material is known, then fractions of each spectral endmember may be obtained by minimizing the sum of squared errors provided there are more equations than unknowns (i.e. more spectral bands than endmembers so that the system of equations is sufficiently determined). Linear Least Squares (LLS) unmixing was applied to the 2004 Landsat image with two to four spectral endmembers and all six reflectance bands (1–5 and 7). The simple two endmember case included only land and water. The three endmember trial included water and split the land endmember into bare and vegetated while the four endmember case also included water and bare while partitioning the vegetated endmember into herbaceous and shrub. Endmember reflectance values were sampled directly from the 2004 Landsat image using orthophotos and Google Earth high resolution imagery when necessary to locate the most homogeneous endmember targets available.

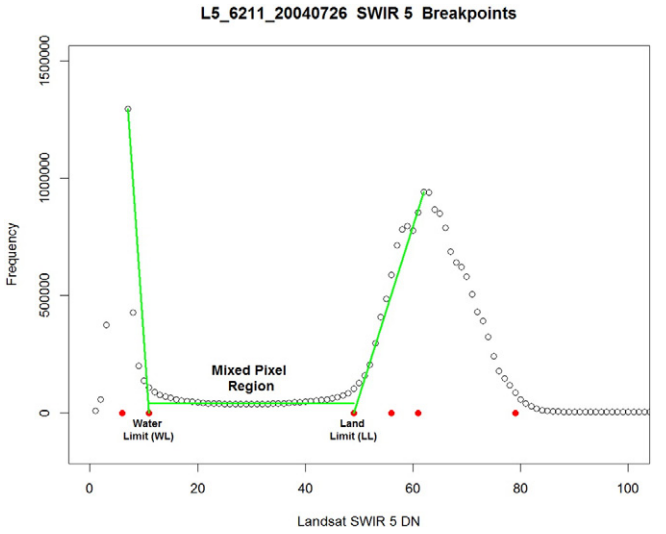

Fig. 3. Typical Landsat Shortwave Infrared band 5 (SWIR 5) frequency histogram of land and water with breakpoint regressions, candidate breakpoints (solid circles) and limits defining the mixed pixel region.

2.3.3. Breakpoint method

Limits of the mixed pixel region can be identified as inflection points (breakpoints) on the SWIR histogram with the water/mixed pixel breakpoint defined as the intersection between decreasing frequency of water pixels with increasing SWIR brightness and the plateau in the mixed pixel region. A second breakpoint corresponding to the darkest pure land pixels is at the intersection between the mixed pixel region and the beginning of the SWIR frequency increase. Points corresponding to the limits of water and land can be identified visually from the histogram or automatically using breakpoint analysis (Fig. 3). Once water and land limits are defined, pixels below the water limit are set to 100% water and those above the land limit to 100% land. Muster et al. (2013) used Landsat 5 to show linear albedo-subpixel water cover (SWC) functions for mixed pixels in three separate tundra environments and state that similar relations should be expected for other Arctic regions. Thus, mixed pixels are interpolated linearly between the two limits using Eq. (1) below:

$$WF\% = (LL - SWIR) \times 100\% / (LL - WL) \quad (1)$$

where:

WF%	Percent water fraction
WL	Water limit
LL	Land limit
SWIR	Landsat band 5 digital number (DN)

Breakpoints were determined using the algorithm described in Bai and Perron (2003) that is implemented in R Statistics, though they may also be obtained from visual inspection of the histogram. Breakpoints were calculated from the SWIR band 5 Digital Numbers

(DNs) histogram for the 2004 scene and were subsequently converted to TOA reflectance to map water fractions from each date in the Landsat image stack. Six candidate breakpoints were initially extracted from which two corresponding to the water and land limits were used.

2.4. Assessment

Landsat water maps for July 26, 2004 generated using the above methods were assessed by comparing them against the August, 2004 orthophoto-based maps using the total water fraction from combined land and water masks and number of pure water pixels. A low percentage error in both water fraction and pure water suggests an accurate representation of lakes and surrounding mixed pixels. Errors were calculated beneath all lake and land masks together, and averages were also computed from errors calculated on 113 individual lakes. Error statistics include overall bias, as well as mean absolute error and average bias of individual lakes.

2.4.1. Analysis of per-pixel water fraction trends

Per-pixel trend images were computed from the stack of 17 Landsat water fraction maps using Theil–Sen regression and Mann–Kendall trend significance on a variable number of observations (mean = 15.13) depending on cloud and shadow masks. Theil–Sen is a robust regression technique whose slope is calculated as the median of all possible pairwise slopes and has been shown to be insensitive to up to 29% outliers. Mann–Kendall trend significance is computed from the number of positive slopes compared to the number of negative slopes in the set of all possible pairwise slopes (Kendall and Stuart, 1967).

The standard deviation of water fraction through time was mapped on a pixel basis to examine inter-annual water variability. The standard deviation was calculated only on pixel water fractions where water was present in two or more dates in the time-series to avoid any cloud shadows classified as water that were missed in the cloud and shadow masks.

3. Results

3.1. Orthophoto water fractions

Orthophoto water fractions aggregated to 30 m beneath the water and surrounding land masks are summarized in Table 2. A total of 13,518 pixels covering 12.17 km^2 consist of pure water within Landsat's 30 m × 30 m pixels. An additional 7037 pixels are mixed at this scale with an average water fraction of 52.36%, providing an extra 3.32 km^2 of surface water area and producing an overall water fraction of 56.36% within the combined land/water masks. This indicates that mixed 30 m pixels account for 21% of the overall surface water area for the lake sample analyzed. These mixed pixels occur around the margins of lakes and do not include mixed water pixels related to other thermokarst features such as ice wedge troughs. Therefore, mixed pixels could potentially account for a significantly higher percentage of the overall water area. It should be noted that these percentages depend on lake shape size, with smaller and more irregularly shaped lakes having a higher percentage of mixed water pixels along shorelines relative to pure pixels.

An examination of the mean area-to-perimeter ratio of the sample of lakes analyzed relative to the population of lakes within the study area is shown in Table 3. A higher ratio is indicative of larger or more regularly shaped lakes with fewer mixed pixels along shorelines. Results show that sample lakes are slightly smaller and/or more irregular than the overall population of lakes, suggesting a higher percentage of mixed pixels in sample lakes. However, the mean area to perimeter ratio of the population is skewed due to a relatively small number of large lakes. Of the nearly 24,000 lakes in the overall population, more than 20,000 are smaller than the average lake size of the sample population and have a mean area to perimeter ratio that is far less than the sample at 29.33 m. Therefore, while all lakes in the overall population have a slightly smaller percentage of mixed pixels than the sample, the majority of them contain a higher percentage of mixed pixels.

In the reference sample, mixed pixels account for approximately one third of all water pixels and water area within mixed pixels represents approximately one fifth of its total water area. In the overall population of lakes on the Tuktoyaktuk Peninsula, the majority contain more edge pixels relative to their area than the sample population. Therefore, an accurate assessment of water area and changes requires a fractional mapping approach at the Landsat scale in order to represent the large percentage of mixed water pixels and the surface water area they contribute to the region.

Table 2
Landsat 30 m × 30 m pixel water fractions of 113 lakes determined from orthophoto classification used to calibrate and validate Landsat water models.

	100% water	Mixed	100% land	Total
N (pixels)	13,518	7037	9967	30,522
Water fraction (%)	100	52.36	0	56.36
Water area (km^2)	12.17	3.32	0	15.48

Table 3
Comparison of area and perimeter of 113 sample lakes relative to the overall population of lakes in the study area.

	N	Area (m^2)	Perimeter (m)	Mean area/perimeter ratio (m)
Sample	113	142,306	1409	67.9
Population	23,995	961,852	1032	73.8

3.2. Results from water extraction methods

As shown previously, all lakes and surrounding land buffers from the orthophotos have a total water fraction of 56.36%, with 13,518, or nearly 44% of pixels consisting of pure water. Statistics reveal strengths and weaknesses of each Landsat water extraction method when assessed against the orthophotos (Table 4). Hard thresholds have already been shown to be sub-optimal at portraying water bodies on the Tuktoyaktuk Peninsula due to the large number of mixed water pixels at the 30 m scale and the high water area that mixed pixels contribute to the overall surface water area. Furthermore, a hard threshold initially set at 26 DN representing the minimum frequency of the SWIR histogram in the mixed pixel region underestimated overall water fraction by 1.8% while overestimating the number of pure water pixels by more than 23%. When the threshold was adjusted to 28 DN to decrease the water fraction bias, the number of pure pixels was further overestimated. Thus, while a reasonable overall water fraction may be obtained by adjusting the threshold, it is achieved by overestimating the number of pure water pixels in the absence of mixed pixels and therefore does

Table 4
Percent water fraction (WF%) and number of pure water pixels beneath a mask that includes 113 reference sample lakes and surrounding land buffers derived from classification of orthophotos (bold). The WF%, number of pure water pixels, and biases are shown below for the different Landsat water extraction methods.

	WF (%)	Bias	100% water pixels	Bias
Ortho	**56.36**	**0.00**	**13,518**	**0**
Breakpoint	56.1	−0.26	13,607	89
Min SWIR threshold DN = <26	54.56	−1.80	16,654	3136
SWIR threshold DN = <28	55.61	−0.75	16,973	3455
SWIR threshold DN = <30	56.67	0.31	17,296	3778
LLS (4EM)	56.26	−0.10	9064	−4454
LLS (3EM)	56.11	−0.25	9061	−4457
LLS (2EM)	65.64	9.28	8687	−4831

not portray a true representation of water. This approach will also lead to varying bias depending on lake size as the ratio of mixed to pure water pixels increases in smaller lakes.

Linear unmixing with different numbers of spectral endmembers achieved the lowest water fraction bias of all methods tested for the three and four endmember cases (−0.25 to −0.1%). Water maps from linear unmixing predicted a maximum water fraction of 118% in all three cases and the number of pure water pixels shown in Table 4 included only those with a fraction equal or greater than 100%. Pure water pixels were greatly underestimated using a 100% threshold, while the overall water fraction was calculated including pixels with values of greater than 100% water. Had pixels predicted to have greater than 100% water been truncated to 100% water prior to calculating the overall water fraction, biases would have been greater in the three and four endmember cases. In the two endmember case, truncating water fraction to 100% reduced the overall water fraction slightly to 64.4% and bias to 8.04%. Similar to hard thresholds, a reasonable overall water fraction is obtained in the three and four endmember cases, but the number of pure pixels is severely underestimated using a 100% threshold as the criterion for pure water pixels.

The breakpoint method performed best overall of the methods tested. The resulting water fraction map underestimated the orthophoto water fraction slightly and was only marginally worse than the best results obtained from LLS. However, unlike LLS that achieved a low bias in overall water fraction by including pixels with greater than 100% water fraction in its calculation, the breakpoint method achieved a similar bias with pure water pixels assigned to 100% water. Further, the number of pure water pixels was also predicted with minimal bias compared to orthophotos. Considering both percent water fraction and number of pure water pixels as evaluation criteria, the breakpoint method depicts water best of all methods tested.

A lake-by-lake comparison led to a similar conclusion to the aggregated comparison above. Hard thresholds produced some of the lowest lake average biases and mean absolute errors of the methods tested, but these were achieved by severely overestimating the number of pure water pixels (Table 5). The fact that biases and mean absolute errors in the number of pure water pixels were identical for the three SWIR thresholds indicates that the number of pure water pixels was overestimated for all 113 lakes. LLS produced higher biases and mean absolute errors in all three cases than hard thresholds for both water fraction and number of pure water pixels. The breakpoint method generated the smallest errors for all measures except for bias in average water fraction, which was second after SWIR threshold DN = <30.

Scatterplots of breakpoint water fraction and number of 100% pure water pixels compared to orthophotos for all 113 reference lakes are shown in Fig. 4 with the 1:1 line in red. At low water fractions, the breakpoint method underestimates the orthophoto water fraction slightly, while overestimating slightly for higher water fractions. The least-squares regression slope is close to one while the offset is only slightly negative, indicating a good 1:1 fit as can be seen from the 1:1 line. Small lakes have a smaller number of pure water pixels than larger lakes and also tend to have a lower water fraction due to a smaller area/perimeter ratio. Large irregularly shaped lakes can also have a relatively low water fraction, however in general, lakes on the low end of the water fraction graph correspond to lakes on the low end of the number of pure water pixels graph. The pure water pixels graph appears similar to the water fraction graph with less underestimation of the breakpoint method for smaller lakes, and overestimation of larger lakes caused by only two lakes with approximately 1000 pure water pixels each.

Table 5
Average water fraction and number of pure 30 m × 30 m water pixels from 113 individual lakes and surrounding land, bias of lake averages and mean absolute errors (MAE).

	WF (%)	bias	MAE	100% water pixels	bias	MAE
Ortho	34.96	0	0	116.37	0	0
Breakpoint	34.59	−0.37	2.69	118.43	2.06	7.35
Min SWIR threshold DN = <26	32.72	−2.24	3.57	145.53	29.16	29.16
SWIR threshold DN = <28	33.84	−1.12	3.04	148.45	32.08	32.08
SWIR threshold DN = <30	34.95	−0.01	2.64	151.38	35.02	35.02
LLS (4EM)	46.09	11.13	11.13	75.82	−40.54	41.69
LLS (3EM)	32.07	−2.89	5.02	79.09	−37.28	38.35
LLS (2EM)	32.44	−2.53	4.75	79.17	−37.20	38.27

3.3. Trend analysis applied to breakpoint water fractions

Table 6 presents a summary of significant trends ($P < 0.05$) for the 17 image stack. The stack includes an average of 15.13 dates per pixel, with different dates included in a pixel's time-series depending on cloud and shadow. The overall area covered by pixels with significant trends is 297 km^2, which is split into significant positive and negative trends with the average trend in percent water fraction per year shown for each. The area of water gained and lost per year is calculated as the product of the number of significantly trended pixels multiplied by average change in water fraction per year. The number of pixels with positive trends is greater than the number with negative trends by a factor of nearly 6. The absolute magnitude of significant positive trends is less than that for negative trends; however, the greater number of pixels with positive trends leads to an overall increase in water of 2.1 km^2 per year. Over the 26 year period covered by the image stack, approximately 15 km^2 of surface water was lost, while 55 km^2 of water area was gained, leading to an overall water increase of more than 40 km^2.

Fig. 5 shows an enlargement of the 17 date trend image for an area directly east of Tuktoyaktuk with significant negative and positive trends at $P < 0.05$.

This area is typical of other regions in continuous permafrost in Alaska, with water fraction increasing at the shoreline margins in the majority of lakes and decreasing in isolated clusters of adjoining lakes due to catastrophic drainage (Jones et al., 2011). Erosion occurs preferentially on northwesterly to north-easterly shorelines, most likely due to dominant winds blowing from the E and NE (Côté & Burn, 2002).

Temporal profiles of water fraction for lake 1 (negative trend — draining) and lakes 2 and 3 (positive trend — expanding) in Fig. 5 are shown in Fig. 6. Different lake drainage mechanisms have been proposed (Mackay, 1988), each with different rates of drainage. Catastrophic or rapid drainage are terms used to describe the process occurring within a few days and up to several weeks (van Everdingen, 1998). Rapid drainage is sudden while lake expansion is shown to be more subtle and progressive. Fig. 6 shows drainage that overall cannot be considered rapid, since it occurred over a period of approximately 12 years from 1993 to 2005 with expansion and further drainage occurring after 2005 until 2011. Episodes within the overall drainage process may have occurred rapidly according to the official definition; however, the temporal resolution of the Landsat stack is insufficient to detect rapid drainage episodes on the order of a few weeks. Expansion of lake 2 along margins is typical of the region and can be seen to be progressive with some inter-annual variation and an absolute increase in water fraction of slightly less than 4% over the 26 year period. Lake 3 may represent the beginnings of thermokarst lake development as most of the lake is expanding and contracting over the over the analysis period with an overall expansion by approximately 34% water fraction.

A histogram of percent change in area of individual lakes can be derived by summing significant water fraction trends within each lake ($n = 21{,}551$) and dividing by lake area. The resulting histogram is positively skewed (Fig. 7), with 74% of lakes showing an overall long-term increase in area, 8% showing a decrease, and 18% showing no net change. If a minimum 25% reduction in lake area is used to define a drained lake (Hinkel et al., 2007), there were 52 lakes larger than 1 ha and 17 lakes larger than 10 ha that drained during the 26-year period between 1985 and 2011.

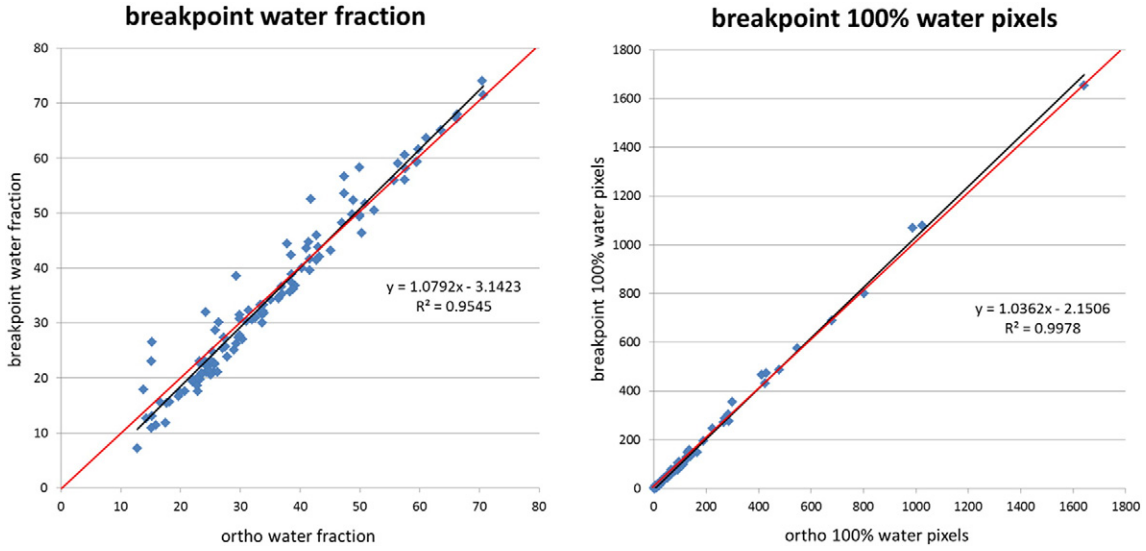

Fig. 4. Scatterplots, least-squares regression and 1:1 lines between orthophoto and Landsat breakpoint water fraction (left) and number of pure water pixels (right) for 113 reference lakes.

3.4. Inter-annual water variability

Fig. 8 shows the Landsat 7 ETM + image from July 23, 2000 in natural color and a gray-scale standard deviation image with significant trends overlaid. Ephemeral water can be seen as a large wetland feature at location 1, some of which is trended positive due to water expansion. Several lakes at location 2 can be seen to be draining as indicated from their significant negative water trends. At location 3 is a lake with wide margins that is wetting and drying on an annual basis due to high water level fluctuations and/or shallow lake margins. All lakes in the region experience a combination of wetting/drying and monotonic expansion along their margins. Note that some of the inter-annual variability within a one-pixel boundary around the lakes may be the result of sub-pixel misregistration shifts among dates. We expect that any image misregistration should be randomly distributed in time and be treated as noise when computing the long-term, per-pixel Theil–Sen trends.

4. Discussion

Other studies that compared approaches to map thermokarst lakes using Landsat include Roach, Griffith and Verbyla (2012) and Rover et al. (2010). Both of these studies were conducted in Alaska's subboreal zone that is sparsely treed, which creates additional challenges for water mapping due to spectral confusion between dark conifer, shadow and water. Roach, Griffith and Verbyla (2012) compared density slicing (thresholding) of Landsat SWIR 5 with classification trees and feature extraction using different Landsat band combinations. They found that while density slicing was as accurate as other methods, it proved to be a better overall approach when considering efficiency, ease of application and the ability to delineate smaller lakes. A direct comparison between their study and ours is difficult to make even though similar methods were tested and reference data were collected from air photo delineation in both cases. The biggest difference between our studies is the way in which reference data were treated and the overall approach that followed. In Roach, Griffith and Verbyla (2012), reference pixels were assigned to either land or water based on a 50% threshold of 30 m pixels overlaid on air photos, and hard classification approaches were trained on these two classes. While not presented here, we tested the same approach and came to similar conclusions about the efficacy and performance of this method. However, in addition to poorly representing the large percentage of mixed pixels in the Tuktoyaktuk region, a binary output is less suitable for trend detection unless continuous fields are calculated at an upscaled, coarser resolution similar to our treatment of 0.5 m air photo classifications upscaled to 30 m fractions. By upscaling a 30 m classification to coarser fractions, the precision of detectable changes is only 30 m. The second study by Rover et al. (2010) obtained a best Root Mean Squared Error (RMSE) of 11% water fraction from Landsat using a regression-tree model assessed against 300 lakes from a 5 m SPOT water map. We calculated a lower RMSE of 3.49% for the breakpoint method over our 113 sample lakes, likely in part because of the absence of trees in our study area.

Our lake change analysis provides a follow-up to the study conducted by Plug et al. (2008) by examining the same region but (1) extending the time series forward by 10 years to 2011, (2) using a denser collection of annual Landsat imagery, and (3) examining both surface water losses and gains in addition to net change. A comparison to that study can be made using the summed water fractions for 10 of 17 dates in the image stack providing consistent, clear-sky coverage over 90% of the study region (Fig. 9). While the trend beneath this mask is not significant at the $P < 0.05$ level mainly due to a single low water year in 2008, a small sample size, and both positive (expansion) and negative (drainage) trends occurring simultaneously in the region, water fraction appears to be trended nonetheless with an increase slightly less than that based on the per-pixel trends. Trends were also calculated for total water fractions beneath the same mask using binary water/land classifications derived from thresholding at less than or equal to 26 DN, or ~6% SWIR reflectance. In this case, the trend magnitude was similar to that obtained using breakpoint fractions at 0.0163% WF/year and the trend slope was also slightly more significant with a 2-sided p-value of 0.0736. Therefore, while the use of fractions enables better mapping

Table 6
Area of Landsat pixel with significant positive and negative Theil–Sen trends using the Mann–Kendall significance test at $P < 0.05$ for an average of 15.13 observations per pixel in the analysis area.

Analysis area (km^2)	17 image stack		
	12,946.8		
	Area of significant pixels (km^2)	% WF/km^2/year	km^2/year
$P < 0.05$ negative trends (drainage)	30	−1.83	−0.5534
$P < 0.05$ positive trends (expansion)	200	1.05	2.0998
$P < 0.05$ all trends	230	0.67	1.55

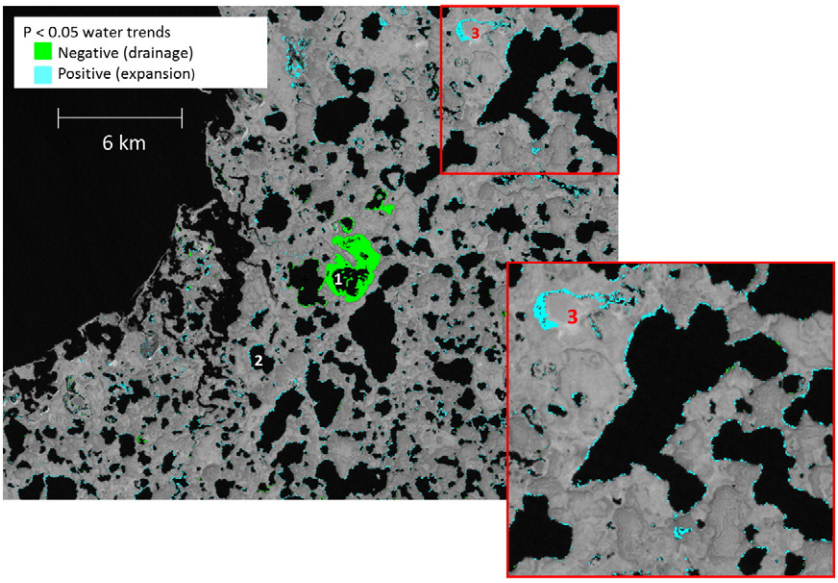

Fig. 5. Significant negative (drainage) and positive (expansion) trends at P < 0.05 overlaid on the 2004 Shortwave Infrared (SWIR 5) Landsat image for an area around the community of Tuktoyaktuk, with an enlarged inset area in red.

and visualization of water changes at resolutions of 30 m or less, both methods produce similar rates of change over the larger region. This suggests that results from previous studies that examined thermokarst water changes using binary classifications should be comparable to results obtained in this study.

Using the breakpoint method, we obtained overall water fractions (~28%) that are comparable to those extracted by Plug et al. (2008) for the Upper Tuktoyaktuk Peninsula. Of the two periods analyzed in Plug et al. (2008), the current analysis overlaps their 1991–1992 to 2000–2001 periods, although the start and end points do not correspond exactly. They noted an absolute decrease in lake area between 2.6 and 2.8% (9–11% relative decrease) on the Lower Peninsula during this period, while our analysis found an absolute water fraction increase of 0.22% between 1992 and 2000 for the 10-date common clear sky area, which corresponds to a 0.64% relative increase. Inter-annual variability in lake area reported in Plug et al. (2008) was 0.3% between 1991 and 1992 and −4% between 2000 and 2001 for a large region of the Central Peninsula. Our analysis suggested variability to be substantially less, as water fraction was found to be nearly stable between 1990 and 1992, varying by 0.11% absolute water fraction or less.

Disparate conclusions between studies may be partly due to different Landsat datasets used to extract water. Plug et al. (2008) used Landsat MSS, TM and ETM + with different sensor characteristics to classify three periods corresponding to the late 1970s, early 1990s and early 2000s. Lake area differences were consistently greatest between MSS for the earliest epoch and TM for the middle epoch, with MSS underestimating lake area compared to TM by upwards of 3%. Recent studies of changing lake extents in Alaska have shown that intra-annual variability during the growing season can be substantial due to the impact of snow melt on water balance (Chen et al., 2014; Roach et al., 2013; Rover et al., 2012). Perhaps a bigger reason for different results between studies was the use of an early summer image (June 28, 1991) by Plug et al. (2008) that may have been partially responsible for the greatest lake area being recorded for the middle of three time periods. In addition, the smaller number of observations employed in Plug et al.'s (2008) analysis consisting of six scenes covering the three dates compared to our 17 scene image stack may have also been partly responsible for differences.

Both MacKay (1988) and Marsh et al. (2009) analyzed historical lake drainage in the same region as the current analysis. Depending on the minimum lake size considered and using a 25% reduction as a minimum threshold for drainage as suggested by Hinkel et al. (2007), our study calculated an average number of drained lakes between 0.65 and 2 per year from 1985 to 2011. Mackay (1988) determined an average

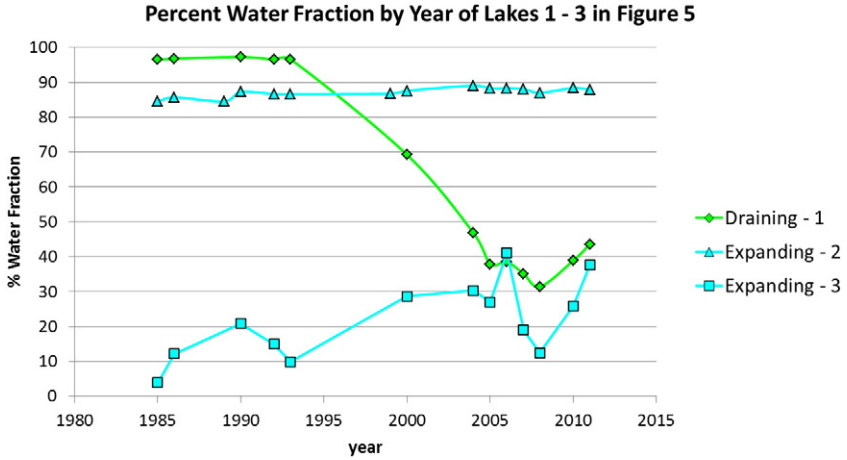

Fig. 6. Annual changes in percent water fraction for draining lake (1) and expanding lakes (2 and 3) in Fig. 4.

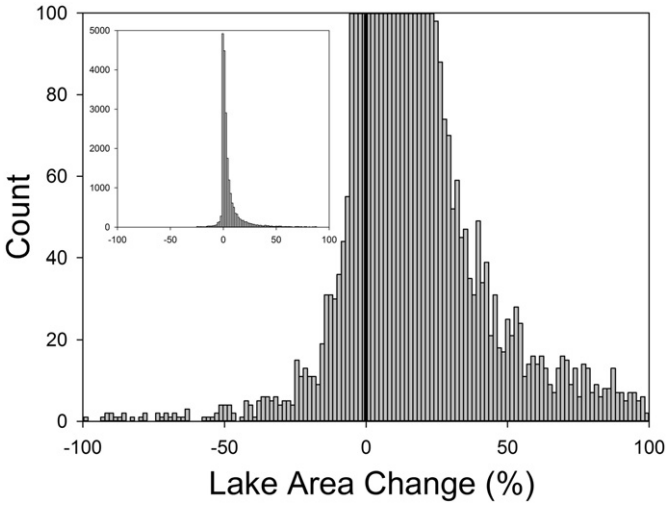

Fig. 7. Frequency histogram of percent lake area change by lake.

drainage rate of 1.81 lakes/year for a similar area over the Tuktoyaktuk Peninsula for the period 1950 to 1986, which suggests a consistent rate between 1950–1986 and 1985–2011 periods. However, Marsh et al. (2009) determined a decreasing rate in the number of lakes drained per year from 1.13 between 1950 and 1973 to approximately 0.33 lakes/year between 1985 and 2006 for an area that was smaller and located just west of the region used in this study.

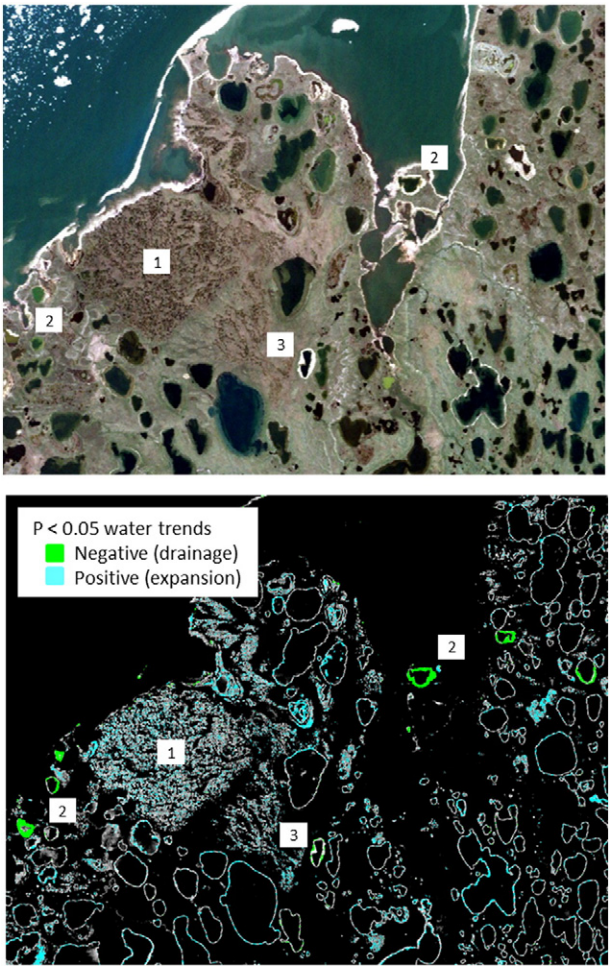

Fig. 8. Per-pixel standard deviation image (bottom) showing relative variation from dark to bright with monotonic significant trends overlain on a portion of the Tuktoyaktuk Peninsula (top) with feature 1. representing a large wetland containing ephemeral water, 2. several draining lakes, and 3. a single lake with wide margins that are both expanding and wetting/drying.

More recently, Lantz and Turner (2015) found that catastrophic lake drainage has become more than five times more frequent in recent decades compared to earlier decades beginning in the 1950s in the Old Crow Flats located approximately 350 km to the southwest of Tuktoyaktuk. For the 1950–1985 period, Marsh et al. (2009) observed a rate of 1.03 lakes/year, which when normalized for differences in area, amounts to an approximate rate of 1.34 lakes/year for an area roughly the size of our and Mackay's (1988) study region. This estimate is slightly low compared to Mackay (1988) for the same time period, however, both study regions do not overlap precisely. Differences may be due to the fact that, according to our analyses, more lakes appear to have drained on the northeastern half of the Peninsula on glaciofluvial and eolian deposits (Rampton, 1987). Discrepancies could also be caused by methods used to identify drained lakes. Both previous studies relied on manual interpretation of air photos at a single point in time to map features caused by drained thaw lake basins (DTLB), which were subsequently verified by looking for a corresponding lake in the previous time period and by field visits. DTLBs that were missed in the interpretation would be omitted from the analyses and there was no means to assess omission error from this approach.

Comparisons between our results and those from other studies in different regions of continuous permafrost reveal more similarities than differences. Smith et al. (2005) noted a 12% increase in lake area in a continuous permafrost region in Western Siberia over a 30 year period between the early 1970s and late 1990s. In Walter et al. (2006), a 14.7% increase in lake area was measured between 1974 and 2000 in North Siberia. In Arp et al. (2011), lake area expansion between 3.2% and 4.1% was noted between 1979 and 2002 for a set of 13 lakes in Alaska's Coastal Plain due to shoreline erosion, while inter-annual variation was explained by precipitation minus evaporation. Jones et al. (2011) found an increase in the size of lakes less than 40 ha in size, but an overall decrease in lake area due to a decrease in the size of a small number of larger lakes caused by drainage between 1978 and 2007 on the Seward Peninsula of Alaska. The nature of changes observed in Jones et al. (2011) is similar to those seen in our analysis with expansion occurring along lake margins throughout and isolated lakes draining. Similarly, Lantz and Turner (2015) determined a decrease in lake area of ~6000 ha in the Yukon's Old Crow Flats, with half of this decrease caused by rapid drainage of a small number of large lakes. However, drainage was the dominant process driving lake area changes in these studies while expansion was dominant in ours. Over a large portion of the Tuktoyaktuk Peninsula, our study is consistent with those above, showing a relative water fraction increase of 6.2% over the 20 year period from 1985 to 2005 before falling to a 4.8% long-term increase by 2011 (Fig. 9). Our observations of long-term expansion of thermokarst lakes are also consistent with a warming-induced, increased rate of retrogressive thaw slump activity adjacent to lakes in the Mackenzie Delta region lying just to the southwest (Lantz & Kokelj, 2008). Warming of ice-rich permafrost and increased ground ice ablation would be expected to accelerate both lake expansion and thaw slumping processes (Plug & West, 2009).

5. Conclusions

The majority of studies we surveyed on regional thermokarst lake change from Landsat relied on binary land/water classifications, while this study demonstrates the need to consider pixel fractions to accurately depict water extent on the Tuktoyaktuk Peninsula in the continuous permafrost zone of Canada's Western Arctic. Hard classification that maps either presence or absence of water also limits change detection to post-classification comparison between two dates, while fractional mapping provides a continuous measure of water that allows regression to assess trends from multiple dates in a time-series. Ultimately, trend

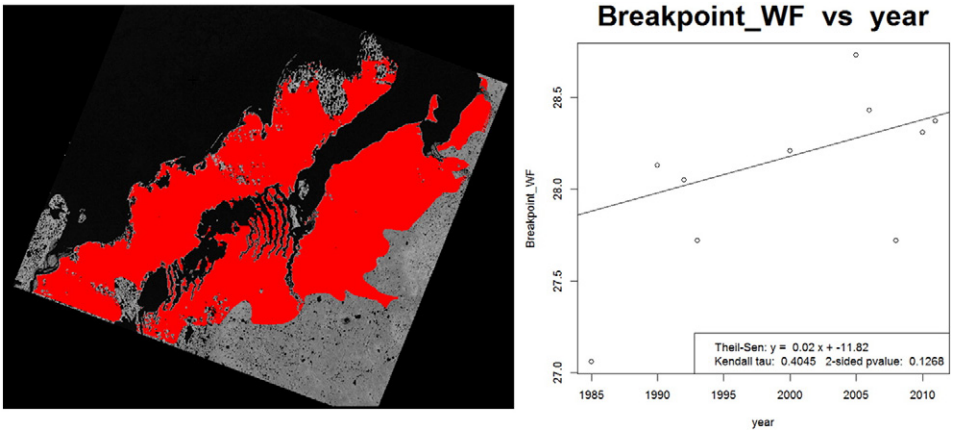

Fig. 9. Thiel–Sen trend in overall water fraction (right) for a common clear-sky area covering 90% of the study region (left) and 10 of 17 dates in the image stack.

detection is more reliable than post-classification comparison because it captures progressive and underlying long-term changes while minimizing the effects of outliers due to anomalous conditions in any single year. Our analysis shows widespread lake expansion on the Tuktoyaktuk Coastal Plain with isolated and episodic lake drainage across the study area at a rate of about two lakes per year. These results are consistent with most other studies in continuous permafrost regions across the pan arctic, with differences attributable to the relative importance of expansion versus drainage in different regions. Future work will examine possible climatic and geological drivers of water extent changes on the Tuktoyaktuk Peninsula, and also in discontinuous permafrost across treeline where additional challenges caused by spectral confusion between water, conifer and tree shadow need to be addressed.

Acknowledgments

Funding for this work was provided by the NWT Cumulative Impacts Monitoring Program (NWT CIMP).

References

The Advanced Theory of Statistics. Vol 2: Inference and Relationship. Second Edition by Kendall, Maurice G. and Alan Stuart: Charles Griffin, London 9780852640111 Hard Cover, 2nd Edition — Peter Rhodes Books. (n.d.). Retrieved October 7, 2014, from http://www.abebooks.co.uk/servlet/BookDetailsPL?bi=10142707302&searchurl=an%3Dkendall%26amp%3Bsortby%3D3%26amp%3Btn%3Dadvanced%2Btheory%2Bof%2Bstatistics.

Arp, C. D., Jones, B. M., Urban, F. E., & Grosse, G. (2011). Hydrogeomorphic processes of thermokarst lakes with grounded-ice and floating-ice regimes on the Arctic coastal plain, Alaska. *Hydrological Processes*, *25*(15), 2422–2438. http://dx.doi.org/10.1002/hyp.8019.

Bai, J., & Perron, P. (2003). Computation and analysis of multiple structural change models. *Journal of Applied Econometrics*, *18*(1), 1–22. http://dx.doi.org/10.1002/jae.659.

Burn, C. R., & Kokelj, S. V. (2009). The environment and permafrost of the Mackenzie Delta area. *Permafrost and Periglacial Processes*, *20*(2), 83–105. http://dx.doi.org/10.1002/ppp.655.

Carroll, M. L., Townshend, J. R. G., DiMiceli, C. M., Loboda, T., & Sohlberg, R. A. (2011). Shrinking lakes of the Arctic: Spatial relationships and trajectory of change. *Geophysical Research Letters*, *38*(20), L20406. http://dx.doi.org/10.1029/2011GL049427.

Chander, G., Markham, B. L., & Helder, D. L. (2009). Summary of current radiometric calibration coefficients for Landsat MSS, TM, ETM+, and EO-1 ALI sensors. *Remote Sensing of Environment*, *113*(5), 893–903. http://dx.doi.org/10.1016/j.rse.2009.01.007.

Chen, M., Rowland, J. C., Wilson, C. J., Altmann, G. L., & Brumby, S. P. (2014). Temporal and spatial pattern of thermokarst lake area changes at Yukon Flats, Alaska. *Hydrological Processes*, *28*(3), 837–852. http://dx.doi.org/10.1002/hyp.9642.

Côté, M. M., & Burn, C. R. (2002). The oriented lakes of Tuktoyaktuk Peninsula, Western Arctic Coast, Canada: A GIS-based analysis. *Permafrost and Periglacial Processes*, *13*(1), 61–70. http://dx.doi.org/10.1002/ppp.407.

Fraser, R. H., Lantz, T. C., Olthof, I., Kokelj, S. V., & Sims, R. A. (2014). Warming-induced shrub expansion and lichen decline in the Western Canadian Arctic. *Ecosystems*, 1–18. http://dx.doi.org/10.1007/s10021-014-9783-3.

Frazier, P. S., & Page, K. J. (2000). Water body detection and delineation with Landsat TM data. *Photogrammetric Engineering and Remote Sensing*, *66*(12), 1461–1467.

Fulton, R. J. (1995). Surficial materials of Canada. Geological Survey of Canada, 'A' Series Map 1880A, 1995. *Natural Resources Canada*. http://dx.doi.org/10.4095/205040.

Heginbottom, J. A., Dubreuil, M. A., & Harker, P. A. (1995). *Canada-permafrost. In National Atlas of Canada, 5th edition*, *Plate 2.1*, Ottawa Canada: Natural Resources Canada (MCR 4177; scale 1:7 500 000).

Hinkel, K. M., Jones, B. M., Eisner, W. R., Cuomo, C. J., Beck, R. A., & Frohn, R. (2007). Methods to assess natural and anthropogenic thaw lake drainage on the western Arctic coastal plain of northern Alaska. *Journal of Geophysical Research, Earth Surface*, *112*(F2), F02S16. http://dx.doi.org/10.1029/2006JF000584.

Hope, A. S., Coulter, L. L., & Stow, D. A. (1999). Estimating lake area in an Arctic landscape using linear mixture modelling with AVHRR data. *International Journal of Remote Sensing*, *20*(2–4), 829–835.

Ji, L., Wylie, B., & Rover, J. (2008). Estimating percent surface-water area using intermediate resolution satellite imagery. *AGU Fall Meeting Abstracts*, *41*, 0874.

Jones, B. M., Grosse, G., Arp, C. D., Jones, M. C., Walter Anthony, K. M., & Romanovsky, V. E. (2011). Modern thermokarst lake dynamics in the continuous permafrost zone, northern Seward Peninsula, Alaska. *Journal of Geophysical Research, Biogeosciences*, *116*(G2), G00M03. http://dx.doi.org/10.1029/2011JG001666.

Kokelj, S. V., & Jorgenson, M. T. (2013). Advances in Thermokarst Research. *Permafrost and Periglacial Processes*, *24*(2), 108–119. http://dx.doi.org/10.1002/ppp.1779.

Lantz, T. C., & Kokelj, S. V. (2008). Increasing rates of retrogressive thaw slump activity in the Mackenzie Delta region, N.W.T., Canada. *Geophysical Research Letters*, *35*(6), L06502. http://dx.doi.org/10.1029/2007GL032433.

Lantz, T. C., & Turner, K. W. (2015). Changes in lake area in response to thermokarst processes and climate in old crow flats, Yukon. *Journal of Geophysical Research, Biogeosciences*. http://dx.doi.org/10.1002/2014JG002744 (2014JG002744).

Mackay, l. R. (1988). Catastrophic lake drainage, Tuktoyaktuk Peninsula area, District of Mackenzie. *Current Research, Part D. Geological Survey of Canada, Paper 88-1D.* (pp. 83–90).

Marsh, P., Russell, M., Pohl, S., Haywood, H., & Onclin, C. (2009). Changes in thaw lake drainage in the Western Canadian Arctic from 1950 to 2000. *Hydrological Processes*, *23*(1), 145–158. http://dx.doi.org/10.1002/hyp.7179.

Muster, S., Heim, B., Abnizova, A., & Boike, J. (2013). Water body distributions across scales: A remote sensing based comparison of three Arctic Tundra wetlands. *Remote Sensing*, *5*(4), 1498–1523. http://dx.doi.org/10.3390/rs5041498.

Plug, L. J., Walls, C., & Scott, B. M. (2008). Tundra lake changes from 1978 to 2001 on the Tuktoyaktuk Peninsula, western Canadian Arctic. *Geophysical Research Letters*, *35*(3), L03502. http://dx.doi.org/10.1029/2007GL032303.

Plug, L. J., & West, J. J. (2009). Thaw lake expansion in a two-dimensional coupled model of heat transfer, thaw subsidence, and mass movement. *Journal of Geophysical Research, Earth Surface*, *114*(F1), F01002. http://dx.doi.org/10.1029/2006JF000740.

Pouliot, D., Latifovic, R., & Olthof, I. (2009). Trends in vegetation NDVI from 1 km AVHRR data over Canada for the period 1985–2006. *International Journal of Remote Sensing*, *30*(1), 149–168. http://dx.doi.org/10.1080/01431160802302090.

Rampton, V.N. (1987). Surficial geology, Tuktoyaktuk Coastlands, District of Mackenzie, Northwest Territories. Geological Survey of Canada, Map 1647A, scale 1:500,000, 1 sheet. doi:10.4095/125160.

Riordan, B., Verbyla, D., & McGuire, A. D. (2006). Shrinking ponds in subarctic Alaska based on 1950–2002 remotely sensed images. *Journal of Geophysical Research, Biogeosciences*, *111*(G4), G04002. http://dx.doi.org/10.1029/2005JG000150.

Roach, J. K., Griffith, B., & Verbyla, D. (2013). Landscape influences on climate-related lake shrinkage at high latitudes. *Global Change Biology*, *19*(7), 2276–2284. http://dx.doi.org/10.1111/gcb.12196.

Roach, J. K., Griffith, B., & Verbyla, D. (2012). Conparison of three methods for long-term monitoring of boreal lake area using Landsat TM and ETM+ imagery. *Canadian Journal of Remote Sensing*, *38*(4), 427–440.

Rover, J., Ji, L., Wylie, B. K., & Tieszen, L. L. (2012). Establishing water body areal extent trends in interior Alaska from multi-temporal Landsat data. *Remote Sensing Letters*, *3*(7), 595–604. http://dx.doi.org/10.1080/01431161.2011.643507.

Rover, J., Wylie, B. K., & Ji, L. (2010). A self-trained classification technique for producing 30 m percent-water maps from Landsat data. *International Journal of Remote Sensing*, *31*(8), 2197–2203. http://dx.doi.org/10.1080/01431161003667455.

Sannel, A. B. K., & Brown, I. A. (2010). High-resolution remote sensing identification of thermokarst lake dynamics in a subarctic peat plateau complex. *Canadian Journal of Remote Sensing, 36*(S1), S26–S40. http://dx.doi.org/10.5589/m10-010.

Serreze, M. C., Walsh, J. E., Iii, F. S. C., Osterkamp, T., Dyurgerov, M., Romanovsky, V., …, & Barry, R. G. (2000). Observational evidence of recent change in the Northern High-Latitude environment. *Climatic Change*, *46*(1–2), 159–207. http://dx.doi.org/10.1023/A:1005504031923.

Singh, A. (1989). Review Article Digital change detection techniques using remotely-sensed data. *International Journal of Remote Sensing, 10*(6), 989–1003. http://dx.doi.org/10.1080/01431168908903939.

Smith, L. C., Sheng, Y., MacDonald, G. M., & Hinzman, L. D. (2005). Disappearing Arctic lakes. *Science (New York, N.Y.)*, *308*(5727), 1429. http://dx.doi.org/10.1126/science.1108142.

Sun, D., Yu, Y., & Goldberg, M. D. (2011). Deriving water fraction and flood maps from MODIS images using a decision tree approach. *IEEE Journal of Selected Topics in Applied Earth Observations & Remote Sensing*, *4*(4), 814–825. http://dx.doi.org/10.1109/JSTARS.2011.2125778.

van Everdingen, Robert (Ed.). (1998). *Revised May 2005. Multi-language glossary of permafrost and related ground-ice terms*. Boulder, CO: National Snow and Ice Data Center.

Vincent, W. F., Laurion, I., Pienitz, R., & Walter Anthony, K. M. (2013). Climate impacts on arctic lake ecosystems. Chapter 2 in Climatic Change and Global Warming of Inland Water: Impacts and Mitigation for Ecosystems and Societies. *First Edition by Charles R. Goldman, Michio Kumagai and Richard D. Robarts*. John Wiley and Sons Ltd.

Walter Anthony, K. M., Zimov, S. A., Grosse, G., Jones, M. C., Anthony, P. M., Iii, F. S. C., …, & Frolking, S. (2014). A shift of thermokarst lakes from carbon sources to sinks during the Holocene epoch. *Nature*, *511*(7510), 452–456. http://dx.doi.org/10.1038/nature13560.

Walter, K. M., Zimov, S. A., Chanton, J. P., Verbyla, D., & Chapin, F. S. (2006). Methane bubbling from Siberian thaw lakes as a positive feedback to climate warming. *Nature*, *443*(7107), 71–75. http://dx.doi.org/10.1038/nature05040.

Weiss, D. J., & Crabtree, R. L. (2011). Percent surface water estimation from MODIS BRDF 16-day image composites. *Remote Sensing of Environment*, *115*(8), 2035–2046. http://dx.doi.org/10.1016/j.rse.2011.04.005.